

Chiral Anomaly and Dynamos from Inhomogeneous Chemical Potential Fluctuations

Jennifer Schober^{1,*}, Igor Rogachevskii^{2,3} and Axel Brandenburg^{3,4,5,6}

¹*Institute of Physics, Laboratory of Astrophysics, École Polytechnique Fédérale de Lausanne (EPFL), 1290 Sauverny, Switzerland*

²*Department of Mechanical Engineering, Ben-Gurion University of the Negev, P.O. Box 653, Beer-Sheva 84105, Israel*

³*Nordita, KTH Royal Institute of Technology and Stockholm University, 10691 Stockholm, Sweden*

⁴*The Oskar Klein Centre, Department of Astronomy, Stockholm University, AlbaNova, SE-10691 Stockholm, Sweden*

⁵*School of Natural Sciences and Medicine, Ilia State University, 0194 Tbilisi, Georgia*

⁶*McWilliams Center for Cosmology and Department of Physics, Carnegie Mellon University, Pittsburgh, Pennsylvania 15213, USA*

 (Received 27 July 2023; revised 19 October 2023; accepted 22 December 2023; published 5 February 2024)

In the standard model of particle physics, the chiral anomaly can occur in relativistic plasmas and plays a role in the early Universe, protoneutron stars, heavy-ion collisions, and quantum materials. It gives rise to a magnetic instability if the number densities of left- and right-handed electrically charged fermions are unequal. Using direct numerical simulations, we show this can result just from spatial fluctuations of the chemical potential, causing a chiral dynamo instability, magnetically driven turbulence, and ultimately a large-scale magnetic field through the magnetic α effect.

DOI: [10.1103/PhysRevLett.132.065101](https://doi.org/10.1103/PhysRevLett.132.065101)

The standard model of particles predicts the occurrence of a macroscopic quantum phenomenon named the “chiral magnetic effect” (CME) [1] in plasmas with high-energy fermions. The CME has been derived using different approaches [2–8]. It implies an electric current along a magnetic field, which arises if there is an asymmetry in the chemical potentials of left- and right-handed fermions, μ_L and μ_R , respectively, i.e., if the chiral chemical potential does not vanish, $\mu_5 \equiv \mu_L - \mu_R \neq 0$. Using chiral magnetohydrodynamics [8–11], it has been shown that the CME leads to chiral dynamo instabilities [12–20], which can amplify the magnetic energy by many orders of magnitude. The CME and the chiral dynamo instabilities have relevance for the early Universe [19–23], protoneutron stars [24–26], quark-gluon plasmas [27–29], heavy-ion collisions [14,15], and for quasiparticles in new materials such as graphene and Dirac semimetals [30]. Recently, it has been shown through direct numerical simulations (DNS) that the chiral dynamo instability occurs not only in systems with initially homogeneous μ_5 , but can develop even from spatial fluctuations of μ_5 with zero mean [31,32]. Producing chiral asymmetry from an initially vanishing μ_5 remains, however, a key question.

In the present study, we demonstrate through DNS that an initially vanishing chiral asymmetry can be produced from an inhomogeneous chemical potential, $\mu = \mu_L + \mu_R$, with just spatial fluctuations ($\nabla\mu \neq 0$). A conversion between μ and μ_5 is possible due to what is known as the chiral separation effect [14,15] and results in a production of large values of μ_5 , which are sufficient for the excitation of a chiral dynamo instability. This leads to the production of magnetically driven turbulence and mean-field

dynamo action, which causes the generation of a large-scale magnetic field.

To study these effects, we consider the following set of equations for an effective description of a plasma composed of chiral electrically charged fermions with the CME and the chiral separation effect:

$$\frac{\partial \mathbf{B}}{\partial t} = \nabla \times [\mathbf{U} \times \mathbf{B} + \eta(\mu_5 \mathbf{B} - \nabla \times \mathbf{B})], \quad (1)$$

$$\rho \frac{D\mathbf{U}}{Dt} = (\nabla \times \mathbf{B}) \times \mathbf{B} - \nabla p + \nabla \cdot (2\nu\rho\mathbf{S}), \quad (2)$$

$$\frac{D\rho}{Dt} = -\rho\nabla \cdot \mathbf{U}, \quad (3)$$

$$\frac{D\mu}{Dt} = -\mu\nabla \cdot \mathbf{U} - C_\mu(\mathbf{B} \cdot \nabla)\mu - \mathcal{D}_\mu \nabla^4 \mu, \quad (4)$$

$$\begin{aligned} \frac{D\mu_5}{Dt} = & -\mu_5\nabla \cdot \mathbf{U} - C_5(\mathbf{B} \cdot \nabla)\mu - \mathcal{D}_5 \nabla^4 \mu_5 \\ & + \lambda\eta[\mathbf{B} \cdot (\nabla \times \mathbf{B}) - \mu_5 \mathbf{B}^2], \end{aligned} \quad (5)$$

where \mathbf{B} and \mathbf{U} are the magnetic and velocity fields, respectively, η is the microscopic magnetic diffusivity, p is the pressure, ν is the viscosity, ρ is the mass density, \mathbf{S} is the trace-free strain tensor with components $S_{ij} = (\partial_j U_i + \partial_i U_j)/2 - \delta_{ij}(\nabla \cdot \mathbf{U})/3$, and $\lambda = 3\hbar c(8\alpha_{\text{em}}/k_B T)^2$ is the chiral feedback parameter. Here, T is the temperature, k_B is the Boltzmann constant, c is the speed of light, $\alpha_{\text{em}} \approx 1/137$ is the fine structure constant, and \hbar is the reduced Planck constant. Equations (1)–(5) are written in Gaussian units and the chemical potentials have been multiplied by a

factor $4\alpha_{\text{em}}/(\hbar c)$ such that they have units of an inverse length [18]. The chiral separation effect is described by the second terms on the rhs of Eqs. (4) and (5). The coupling between μ_5 and μ , determined by the value of the constants C_5 and C_μ , leads to chiral magnetic waves (CMWs) with the frequency $\omega_{\text{CMW}} \approx \pm(C_5 C_\mu)^{1/2} k_\mu |\mathbf{B}|$ [33], where k_μ is the inverse length scale over which μ changes along the magnetic field \mathbf{B} . For numerical stability, the evolution equations for μ_5 and μ also include artificial (hyper-)diffusion terms with small diffusion coefficients \mathcal{D}_5 and \mathcal{D}_μ , respectively [32].

For our numerical analysis, we use the Pencil Code [34] and solve Eqs. (1)–(5) in a three-dimensional periodic domain of size L^3 with a resolution of up to $N^3 = 1024^3$ mesh points. This code employs a third-order accurate time-stepping method [35] and sixth-order explicit finite differences in space [36,37]. The numerical domain ranges from the minimum wave number $k_1 = 2\pi/L$ up to the Nyquist wave number $k_{\text{Ny}} = Nk_1/2$. We use an isothermal equation of state with $p = \rho c_s^2$, where c_s is the sound speed. The density is initially uniform and, because of mass conservation, its value is always equal to the mean density $\langle \rho \rangle$, where angle brackets denote averaging. In the following, we set $k_1 = c_s = \langle \rho \rangle = 1$. For the magnetic Prandtl number, $\text{Pr}_M = \nu/\eta$, we choose $\text{Pr}_M = 1$, and \mathcal{D}_5 and \mathcal{D}_μ are chosen such that the dissipation rates of μ_5 and μ equal the ones of \mathbf{B} and \mathbf{U} at $k = k_{\text{Ny}}$. In our analysis, time is either normalized by the diffusion time, $t_\eta = (\eta k_1^2)^{-1} = \eta^{-1}$, or by the period of the CMW, $t_{\text{CMW}} = 2\pi/\omega_{\text{CMW}}$.

Fluctuations of μ at the initial time t_0 are chosen as Gaussian noise with a power spectrum $E_\mu(k)$, i.e., $E_\mu(k, t_0) = E_{\mu,0} k^s$. Here, $E_\mu(k)$ is normalized such that $\int E_\mu(k) dk = \langle \mu^2 \rangle$. The amplitude $E_{\mu,0}$ is chosen such that the maximum values of μ are comparable for all runs at the time of the onset of the small-scale chiral instability. To allow for chiral magnetic waves in the simulations, we apply a small external magnetic field $\mathbf{B}_{\text{ex}} = (B_{\text{ex}}, 0, 0)$, which effectively produces the chiral anomaly. We further consider a zero initial velocity field \mathbf{U} and weak perturbations of the initial magnetic field \mathbf{B} in the form of Gaussian noise. A summary of runs discussed in this Letter is given in Table I, where $\text{Re}_M = U_{\text{rms}}/(k_{\text{int}}\eta)$ is the magnetic Reynolds number, $\text{Lu} = U_{\text{A,rms}}/(k_{\text{int}}\eta)$ is the Lundquist number, U_{rms} is the rms of the velocity fluctuations, and $U_{\text{A,rms}}$ is the Alfvén speed based on the rms magnetic

TABLE I. Summary of the simulations.

Run	Res.	$C_5 = C_\mu$	λ	Maximum value of			
				$\mu_{5,\text{max}}$	B_{rms}	Re_M	Lu
R1	1024^3	3	4×10^2	68	0.12	77	440
R2	672^3	10	4×10^4	38	0.024	36	98

fluctuations. Further, $k_{\text{int}}^{-1} = \mathcal{E}_M^{-1} \int k^{-1} E_M(k) dk$ is the integral scale of the magnetically driven turbulence, where $E_M(k)$ is the magnetic energy spectrum with its peak close to k_{int} and $\mathcal{E}_M = \langle \mathbf{B}^2 \rangle / 2 = \int E_M(k) dk$ is the turbulent magnetic energy density.

Whether enough chiral asymmetry can be produced to trigger the chiral dynamo instability depends on the characteristic timescales of the system [38]. In particular, the chiral dynamo instability needs to occur on a time-scale shorter than half the period t_{CMW} of the CMW, $t_{\text{CMW}}/2 = \pi/\omega_{\text{CMW}}$. Otherwise, when $t > t_{\text{CMW}}/2$, the chiral chemical potential changes its sign in the CMW, and the chiral dynamo instability starts again. Here, for a linear CMW, the maximum value that μ_5 can reach is approximately the initial value of μ , i.e., $\max(\mu_{5,\text{max}}) = \mu_{\text{max}}(t_0)$. In this Letter, we focus on times $t < t_{\text{CMW}}$.

The different stages of chiral asymmetry production and magnetic field amplification are shown in Fig. 1. In Phase 1, a chiral asymmetry is produced via the second term on the rhs in Eq. (5). For times less than the period of the CMW, i.e., $t \ll t_{\text{CMW}}$ and as long as B_{ex} dominates over magnetic fluctuations, the evolution of μ_5 is described as

$$|\mu_5(t)| \approx C_5 |(\mathbf{B} \cdot \nabla) \mu(t)| t \approx C_5 |B_{\text{ex}} k_{\mu,\text{eff}}(t_0) \mu(t_0)| t, \quad (6)$$

where $k_{\mu,\text{eff}}$ is the characteristic wave number of the initial μ . Introducing the spectrum of the chiral chemical potential $E_5(k)$ as $\int E_5(k) dk = \langle \mu_5^2 \rangle$, and using the estimate for $|\mu_5(t)|$ given by Eq. (6), we relate the spectrum functions $E_5(k)$ and $E_\mu(k)$ as $[E_5(k)k]^{1/2} \approx C_5 B_{\text{ex}} k [E_\mu(k)k]^{1/2} t$. Hence, initial spatial fluctuations of the chemical potential with a spectrum $E_\mu(k) \propto k^s$ produce fluctuations of the chiral chemical potential with the spectrum

$$E_5(k) \propto k^{2+s} t^2. \quad (7)$$

The time evolution determined by Eq. (6) is seen in the initial times of Runs R1 and R2 [see Fig. 2(a)]. Moreover, the obtained spectrum $E_5(k)$ in Phase 1 of Run R2 is $\propto k^{-2}$ [see Fig. 3(b)], as expected from Eq. (7), where the initial

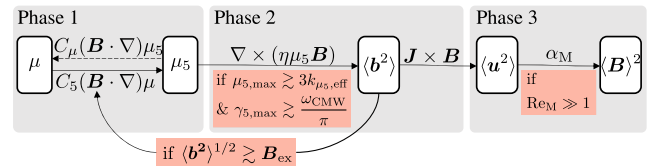


FIG. 1. Illustration of the dynamics in a plasma with autonomous production of chiral asymmetry (Phase 1), accompanied by a generation of fluctuations in the magnetic field $\langle b^2 \rangle^{1/2}$ (Phase 2) and the velocity field $\langle u^2 \rangle^{1/2}$. If the magnetic Reynolds number becomes larger than unity, the magnetic α effect produces a large-scale magnetic field $\langle B \rangle$ (Phase 3).

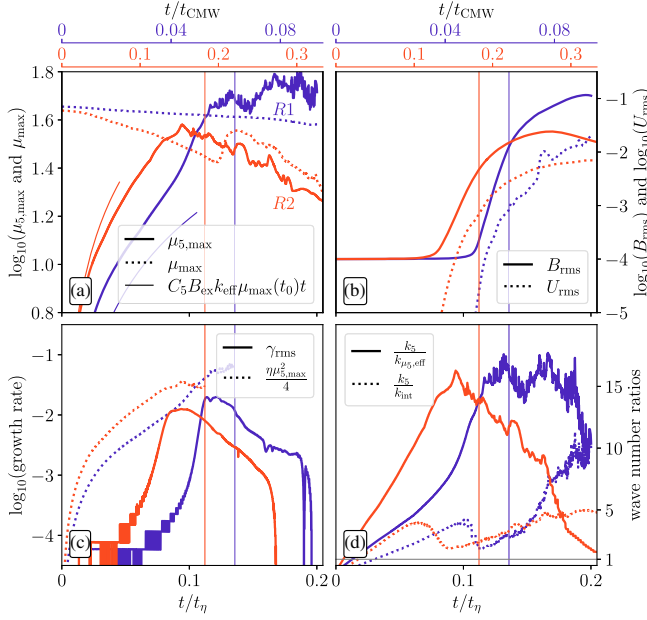


FIG. 2. Comparison of Runs R1 (blues lines) and R2 (red lines). (a) Time evolution of the maximum values of μ_5 (solid lines) and μ (dotted lines). (b) Time evolution of B_{rms} (solid lines) and U_{rms} (dotted lines). (c) Time evolution of the measured growth rate of B_{rms} , γ_{rms} (solid lines), and comparison with the theoretical expectation for the chiral dynamo instability (dotted lines). (d) Time evolution of the ratio of the wave number k_5 , on which the chiral dynamo instability occurs, over the effective correlation wave number $k_{\mu_5, \text{eff}}$ of μ_5 . Thin vertical lines indicate the respective times when the magnetic Reynolds number Re_M becomes larger than unity.

spectrum of the chemical potential has the exponent $s = -4$; see Fig. 3(a).

Phase 2 starts when μ_5 exceeds a critical value for the excitation of the chiral dynamo instability, resulting in exponential growth of magnetic fluctuations. The growth rate of this instability is estimated as

$$\gamma(k) \approx \eta \mu_{5, \text{max}} k - \eta k^2, \quad (8)$$

where $\mu_{5, \text{max}}$ is the spatial maximum of μ_5 [31,32]. The maximum possible growth rate is

$$\gamma_5(t) = \eta \mu_{5, \text{max}}^2(t)/4, \quad (9)$$

but it is only reached when the instability wave number $k_5(t) = \mu_{5, \text{max}}(t)/2$, is much larger than the effective correlation wave number of the fluctuations of μ_5

$$k_{\mu_5, \text{eff}}^{-1}(t) = \langle \mu_5^2 \rangle^{-1} \int k^{-1} E_5(k) dk. \quad (10)$$

The latter condition applies only to systems in which the initial μ or μ_5 are dominated by fluctuations [31,32].

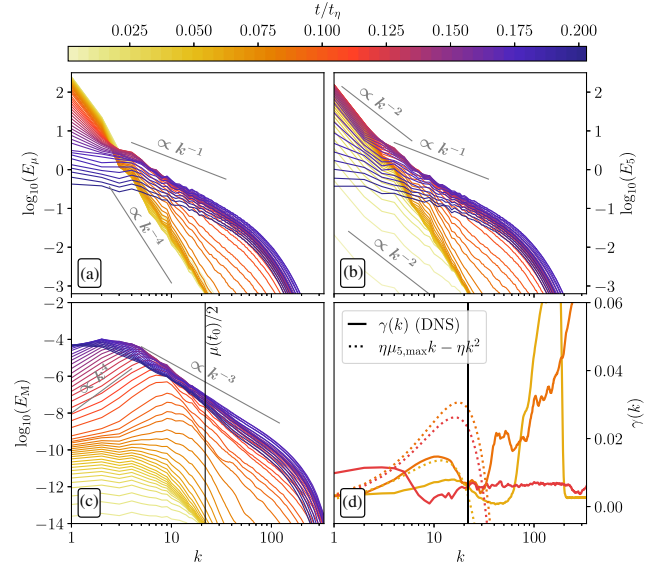


FIG. 3. Evolution of spectra for Run R2 with the time indicated by the color bar. (a) Spectrum $E_\mu(k)$ of μ . (b) Spectrum $E_5(k)$ of μ_5 . (c) Magnetic energy spectrum $E_M(k)$. (d) Growth rate of the magnetic field strength as a function of wave number, $\gamma(k)$ (solid lines) for three different times ($t/t_\eta = 0.06, 0.09$, and 0.12), and theoretically expected growth rate (dotted lines). The thin vertical lines indicate the wave number of the chiral dynamo instability if the initial μ were completely converted into μ_5 .

The time evolution of the rms magnetic field (B_{rms}), the measured growth rate of B_{rms} (γ_{rms}), and the ratio $k_5/k_{\mu_5, \text{eff}}$ are shown in Fig. 2 for Runs R1 and R2. We find that the maximum growth rate of the chiral dynamo instability is attained when the scale separation ratio obeys $k_5/k_{\mu_5, \text{eff}} \gtrsim 10$, as can be seen when comparing Figs. 2(c) and 2(d). In Fig. 3(d), we show the measured growth rate of the scale-dependent magnetic field strength and compare it with the rough estimate for the growth rate given by Eq. (9) for three instants during Phase 2. While the measured curves $\gamma(k)$ do have a peak at higher k initially, they become more and more flat with time, indicating efficient mode coupling. Such a k -independent growth rate has also been observed in simulations of chiral magnetohydrodynamics (MHD) with a spatially homogeneous μ_5 when turbulence is driven by an artificial forcing term in the Navier-Stokes equation [16] and in the kinematic stage of a helically driven large-scale dynamo in classical MHD [39]. Note, that during Phase 2, μ_5 continues to grow, and the field B_{ex} is being replaced by $B_{\text{ex}} + b(t)$, once $b(t) \gtrsim B_{\text{ex}}$, where b are magnetic fluctuations. Therefore, the μ_5 production phase becomes nonlinear. For Run R1, the transition to the nonlinear chiral asymmetry production phase occurs at $t \approx 0.1t_\eta$; see Fig. 2(a).

Eventually, the chiral dynamo instability reaches its nonlinear stage since the Lorentz force [the first term on the rhs of Eq. (2)] increases with time due to the nonlinear evolution of the magnetic field. The Lorentz force produces

velocity fluctuations [see Fig. 2(b)], and the fluid and magnetic Reynolds numbers become larger than unity. Thus, Phase 3 begins, magnetically dominated turbulence is produced, and a large-scale magnetic field is generated via a mean-field dynamo instability, which is excited with the growth rate

$$\gamma_\alpha = (\eta\langle\mu_5\rangle + \alpha_M)k - (\eta + \eta_T)k^2. \quad (11)$$

Here, $\alpha_M = 2(q-1)/(q+1)\tau_c\chi_c$ is the magnetic α effect, which is determined by the current helicity $\chi_c = \langle\mathbf{b}\cdot(\nabla\times\mathbf{b})\rangle \approx \langle\mathbf{a}\cdot\mathbf{b}\rangle k_{\text{int}}^2$, where q is the exponent of the magnetic energy spectrum $E_M \propto k^{-q}$, and $\langle\mu_5\rangle$ is the mean chiral chemical potential. As follows from Fig. 3(c), the exponent is $q \approx 3$. The correlation time of the magnetically driven turbulence is $\tau_c \approx (U_A k_{\text{int}})^{-1}$, where the Alfvén speed is $U_A = \sqrt{\langle\mathbf{b}^2\rangle} \approx B_{\text{rms}}$. The mean fluid density $\langle\rho\rangle$ entering in U_A and α_M is set to unity. The turbulent diffusion coefficient η_T is estimated as $\eta_T = U_{\text{rms}}/(3k_{\text{int}})$. The growth rate γ_α of the mean-field dynamo instability attains the maximum value

$$\gamma_\alpha^{\text{max}} = \frac{(\eta\langle\mu_5\rangle + \alpha_M)^2}{4(\eta + \eta_T)}. \quad (12)$$

The current helicity χ_c and magnetic α effect α_M can also be estimated from the evolutionary equation for the magnetic helicity $\langle\mathbf{a}\cdot\mathbf{b}\rangle$ of the small-scale field $\mathbf{b} = \nabla\times\mathbf{a}$ in chiral MHD [10]:

$$\begin{aligned} \frac{\partial}{\partial t}\langle\mathbf{a}\cdot\mathbf{b}\rangle + \nabla\cdot\mathbf{F} &= 2\eta\langle\mu_5\rangle\langle\mathbf{b}^2\rangle - 2\langle\mathcal{E}\rangle\cdot\langle\mathbf{B}\rangle \\ &\quad - 2\eta\langle\mathbf{b}(\nabla\times\mathbf{b})\rangle, \end{aligned} \quad (13)$$

where \mathbf{F} is the flux of $\langle\mathbf{a}\cdot\mathbf{b}\rangle$ and $\langle\mathcal{E}\rangle \equiv \langle\mathbf{u}\times\mathbf{b}\rangle = \alpha_M\langle\mathbf{B}\rangle - \eta_T(\nabla\times\langle\mathbf{B}\rangle)$ is the turbulent electromotive force. In the steady-state, two leading source or sink terms in Eq. (13), $2\eta\langle\mu_5\rangle\langle\mathbf{b}^2\rangle - 2\alpha_M\langle\mathbf{B}\rangle^2$, compensate each other, so that the magnetic α effect reaches $\alpha_M^{\text{sat}} = \eta\langle\mu_5\rangle\langle\mathbf{b}^2\rangle/\langle\mathbf{B}\rangle^2$ [31,32].

We present an analysis of the mean-field dynamo stage for Runs *R1* and *R2* in Fig. 4. In our system, where velocity fluctuations are driven by an increasing Lorentz force during the nonlinear phase of the chiral dynamo instability, the integral scale of turbulence, k_{int}^{-1} , increases with time. This implies that the turbulent range of scales is expanding in time. To take this fact into account, we perform averaging over the scales larger than k_{int}^{-1} at a given time. In particular, the mean quantities used in Fig. 4 are calculated in the simulations as $\langle\mathbf{B}\rangle_{\text{int}} \equiv [2\int E_M(k)f(k)dk]^{1/2}$, $\langle\mu_5\rangle_{\text{int}} \equiv [\int E_5(k)f(k)dk]^{1/2}$, and $\langle\mathbf{A}\cdot\mathbf{B}\rangle_{\text{int}} \equiv \int H_M(k)f(k)dk$, where $f(k) = [1 - \tanh(k - k_{\text{int}})]/2$ and $H_M(k)$ is the magnetic helicity spectrum. From these averages we calculate $\alpha_{M,\text{int}} = \langle\mathbf{A}\cdot\mathbf{B}\rangle_{\text{int}}k_{\text{int}}/B_{\text{rms}}$ and $\alpha_{M,\text{int}}^{\text{sat}} = \eta\langle\mu_5\rangle_{\text{int}}B_{\text{rms}}^2/\langle\mathbf{B}\rangle_{\text{int}}^2$. As can be seen in

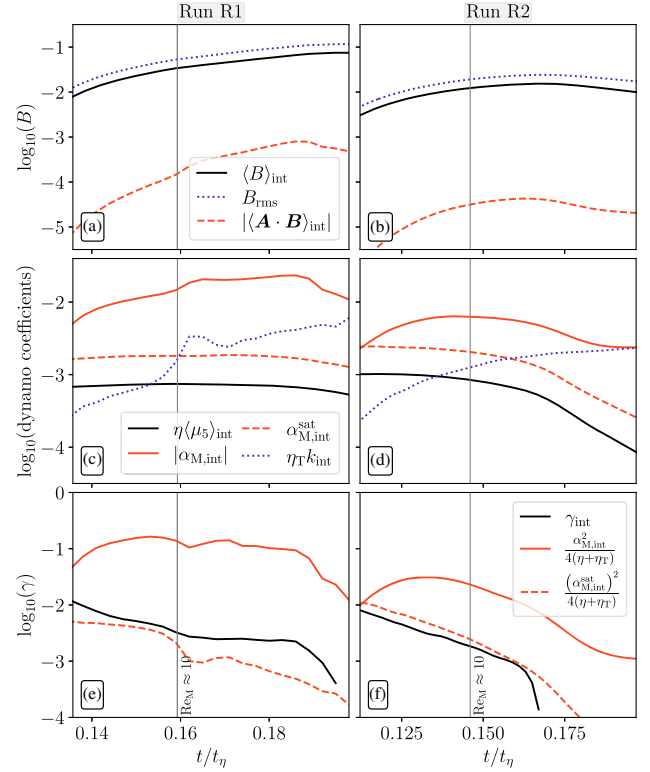


FIG. 4. Mean-field analysis for Runs *R1* (left panels) and *R2* (right panels). (a),(b) Time evolution of the mean magnetic field $\langle\mathbf{B}\rangle_{\text{int}}$ (black lines), B_{rms} (dotted blue lines), magnetic helicity $\langle\mathbf{A}\cdot\mathbf{B}\rangle_{\text{int}}$ (dashed red lines). (c),(d) Time evolution of $\eta\langle\mu_5\rangle_{\text{int}}$ (black lines), $\alpha_{M,\text{int}}$ (red lines), and $\eta_T k_{\text{int}}^2$ (dotted blue lines). (e),(f) Time evolution of the growth rate γ_{int} (black solid line) of $\langle\mathbf{B}\rangle_{\text{int}}$ compared to the mean-field dynamo prediction, where the maximum growth rate is based on $\alpha_{M,\text{int}}$ (solid red line) and $\alpha_{M,\text{int}}^{\text{sat}}$ (dashed red line). The time evolution presented here starts at the time when Re_M exceeds unity and thin vertical lines indicate when Re_M becomes larger than 10.

panels (e) and (f) of Fig. 4, the measured growth rate of the mean magnetic field is comparable with the theoretical predictions based on the magnetic α effect. In the mean-field dynamo phase, the dynamo generation term $\alpha_{M,\text{int}}^{\text{sat}}k_{\text{int}}$ is larger than the damping term $\eta_T k_{\text{int}}^2$. However, since the level of turbulence increases, the turbulent diffusion coefficient η_T increases and $\alpha_{M,\text{int}}^{\text{sat}}$ decreases, leading finally to the end of the mean-field dynamo instability.

Since α_M and η_T change in time in the simulations, Eqs. (11) and (12) serve only as rough estimates on the order of magnitude for the growth rates of the mean-field dynamo instability used for comparisons with DNS. A similar statement is also valid for Eqs. (8) and (9) for the growth rates of the chiral dynamo instability used for comparisons with DNS.

The dynamo instability can, in principle, be followed by an inverse cascade of magnetic energy that is related to a conservation law. In chiral MHD, the total chirality (the sum of the chiral chemical potential and the magnetic

helicity multiplied by $\lambda/2$) is conserved. In this study, both the initial magnetic helicity and the chiral chemical potential vanish, so the anomaly-induced inverse cascade related to the decrease of chiral chemical potential due to the increase of magnetic helicity during the nonlinear chiral dynamo (as described in [20]) is not present. However, it has been shown that in chiral MHD with vanishing total chirality an adaptation of the Hosking integral [40] is conserved [41], which leads to an increase of the magnetic correlation length during the decay of magnetic energy. In our present study, such a long-term evolution cannot be studied because at dynamo saturation the magnetic correlation length has already reached the size of the numerical domain.

In conclusion, we have found a scenario in which a chiral asymmetry is produced in a plasma with initially balanced numbers of left- and right-handed electrically charged fermions due to the joint action of the chiral separation effect and spatial inhomogeneity in fluctuations of the chemical potential. This causes a chiral dynamo instability and the subsequent production of magnetically driven turbulence followed by large-scale magnetic field generation through the magnetic α effect. This scenario can be relevant for the early Universe if chirality is not produced by other mechanisms. It might be less relevant for proto-neutron stars since a net chiral chemical potential can there be produced due to neutrino emission [42]. Beyond astrophysics, this scenario might also be relevant for condensed matter systems.

This study was initiated several years ago through productive discussions with Dmitry Kharzeev. J.S. acknowledges the support from the Swiss National Science Foundation under Grant No. 185863. A.B. was supported in part through a grant from the Swedish Research Council (Vetenskapsrådet, 2019-04234). Nordita was sponsored by NordForsk. We acknowledge the allocation of computing resources provided by the Swedish National Allocations Committee at the Center for Parallel Computers at the Royal Institute of Technology in Stockholm.

*Corresponding author: jennifer.schober@epfl.ch

- [1] A. Vilenkin, Equilibrium parity violating current in a magnetic field, *Phys. Rev. D* **22**, 3080 (1980).
- [2] A. N. Redlich and L. C. R. Wijewardhana, Induced Chern-Simons terms at high temperatures and finite densities, *Phys. Rev. Lett.* **54**, 970 (1985).
- [3] K. Tsokos, Topological mass terms and the high temperature limit of chiral gauge theories, *Phys. Lett.* **157B**, 413 (1985).
- [4] J. Fröhlich and B. Pedrini, New applications of the chiral anomaly, in *Mathematical Physics 2000, International Conference on Mathematical Physics 2000, Imperial College (London)*, edited by A. S. Fokas, A. Grigoryan, T. Kibble, and B. Zegarlinski (World Scientific Publishing Company, Singapore, 2000).
- [5] J. Fröhlich and B. Pedrini, Axions, quantum mechanical pumping, and primeval magnetic fields, in *Statistical Field Theory*, edited by A. Cappelli and G. Mussardo (Springer, Dordrecht, 2002).
- [6] K. Fukushima, D. E. Kharzeev, and H. J. Warringa, The chiral magnetic effect, *Phys. Rev. D* **78**, 074033 (2008).
- [7] D. T. Son and P. Surowka, Hydrodynamics with triangle anomalies, *Phys. Rev. Lett.* **103**, 191601 (2009).
- [8] A. Y. Alekseev, V. V. Cheianov, and J. Fröhlich, Universality of transport properties in equilibrium, the Goldstone theorem, and chiral anomaly, *Phys. Rev. Lett.* **81**, 3503 (1998).
- [9] M. Giovannini, Anomalous magnetohydrodynamics, *Phys. Rev. D* **88**, 063536 (2013).
- [10] I. Rogachevskii, O. Ruchayskiy, A. Boyarsky, J. Fröhlich, N. Kleeorin, A. Brandenburg, and J. Schober, Laminar and turbulent dynamos in chiral magnetohydrodynamics. I. Theory, *Astrophys. J.* **846**, 153 (2017).
- [11] K. Hattori, Y. Hirono, H.-U. Yee, and Y. Yin, Magnetohydrodynamics with chiral anomaly: Phases of collective excitations and instabilities, *Phys. Rev. D* **100**, 065023 (2019).
- [12] A. Boyarsky, J. Fröhlich, and O. Ruchayskiy, Magnetohydrodynamics of chiral relativistic fluids, *Phys. Rev. D* **92**, 043004 (2015).
- [13] D. Grabowska, D. B. Kaplan, and S. Reddy, Role of the electron mass in damping chiral plasma instability in Supernovae and neutron stars, *Phys. Rev. D* **91**, 085035 (2015).
- [14] D. E. Kharzeev, The chiral magnetic effect and anomaly-induced transport, *Prog. Part. Nucl. Phys.* **75**, 133 (2014).
- [15] D. E. Kharzeev, J. Liao, S. A. Voloshin, and G. Wang, Chiral magnetic and vortical effects in high-energy nuclear collisions—A status report, *Prog. Part. Nucl. Phys.* **88**, 1 (2016).
- [16] J. Schober, I. Rogachevskii, A. Brandenburg, A. Boyarsky, J. Fröhlich, O. Ruchayskiy, and N. Kleeorin, Laminar and turbulent dynamos in chiral magnetohydrodynamics. II. Simulations, *Astrophys. J.* **858**, 124 (2018).
- [17] J. Schober, A. Brandenburg, I. Rogachevskii, and N. Kleeorin, Energetics of turbulence generated by chiral MHD dynamos, *Geophys. Astrophys. Fluid Dyn.* **113**, 107 (2019).
- [18] J. Schober, A. Brandenburg, and I. Rogachevskii, Chiral fermion asymmetry in high-energy plasma simulations, *Geophys. Astrophys. Fluid Dyn.* **114**, 106 (2020).
- [19] M. Joyce and M. Shaposhnikov, Primordial magnetic fields, right electrons, and the Abelian anomaly, *Phys. Rev. Lett.* **79**, 1193 (1997).
- [20] A. Boyarsky, J. Fröhlich, and O. Ruchayskiy, Self-consistent evolution of magnetic fields and chiral asymmetry in the early universe, *Phys. Rev. Lett.* **108**, 031301 (2012).
- [21] A. Boyarsky, O. Ruchayskiy, and M. Shaposhnikov, Long-range magnetic fields in the ground state of the Standard Model plasma, *Phys. Rev. Lett.* **109**, 111602 (2012).
- [22] M. Dvornikov and V. B. Semikoz, Influence of the turbulent motion on the chiral magnetic effect in the early universe, *Phys. Rev. D* **95**, 043538 (2017).
- [23] A. Brandenburg, J. Schober, I. Rogachevskii, T. Kahniashvili, A. Boyarsky, J. Fröhlich, O. Ruchayskiy,

- and N. Kleeorin, The turbulent chiral-magnetic cascade in the early universe, *Astrophys. J. Lett.* **845**, L21 (2017).
- [24] M. Dvornikov and V.B. Semikoz, Generation of the magnetic helicity in a neutron star driven by the electroweak electron-nucleon interaction, *J. Cosmol. Astropart. Phys.* **05** (2015) 032.
- [25] N. Yamamoto, Scaling laws in chiral hydrodynamic turbulence, *Phys. Rev. D* **93**, 125016 (2016).
- [26] G. Sigl and N. Leite, Chiral magnetic effect in protoneutron stars and magnetic field spectral evolution, *J. Cosmol. Astropart. Phys.* **01** (2016) 025.
- [27] Y. Akamatsu and N. Yamamoto, Chiral plasma instabilities, *Phys. Rev. Lett.* **111**, 052002 (2013).
- [28] Y. Hirono, D. E. Kharzeev, and Y. Yin, Self-similar inverse cascade of magnetic helicity driven by the chiral anomaly, *Phys. Rev. D* **92**, 125031 (2015).
- [29] S. F. Taghavi and U. A. Wiedemann, Chiral magnetic wave in an expanding QCD fluid, *Phys. Rev. C* **91**, 024902 (2015).
- [30] V. A. Miransky and I. A. Shovkovy, Quantum field theory in a magnetic field: From quantum chromodynamics to graphene and dirac semimetals, *Phys. Rep.* **576**, 1 (2015).
- [31] J. Schober, I. Rogachevskii, and A. Brandenburg, Production of a chiral magnetic anomaly with emerging turbulence and mean-field dynamo action, *Phys. Rev. Lett.* **128**, 065002 (2022).
- [32] J. Schober, I. Rogachevskii, and A. Brandenburg, Dynamo instabilities in plasmas with inhomogeneous chiral chemical potential, *Phys. Rev. D* **105**, 043507 (2022).
- [33] D. E. Kharzeev and H.-U. Yee, Chiral magnetic wave, *Phys. Rev. D* **83**, 085007 (2011).
- [34] A. Brandenburg *et al.* (Pencil Code Collaboration), The Pencil Code, a modular MPI code for partial differential equations and particles: multipurpose and multiuser-maintained, *J. Open Source Software* **6**, 2807 (2021).
- [35] J. H. Williamson, Low-storage Runge-Kutta schemes, *J. Comp. Physiol.* **35**, 48 (1980).
- [36] A. Brandenburg and W. Dobler, Hydromagnetic turbulence in computer simulations, *Comput. Phys. Commun.* **147**, 471 (2002).
- [37] A. Brandenburg, Computational aspects of astrophysical mhd and turbulence, in *Advances in Nonlinear Dynamics*, edited by A. Ferriz-Mas and M. Núñez (Taylor & Francis, London, New York, 2003), pp. 269–344.
- [38] J. Schober, I. Rogachevskii, and A. Brandenburg, Efficiency of dynamos from autonomous generation of chiral asymmetry (unpublished).
- [39] K. Subramanian and A. Brandenburg, Traces of large-scale dynamo action in the kinematic stage, *Mon. Not. R. Astron. Soc.* **445**, 2930 (2014).
- [40] D. N. Hosking and A. A. Schekochihin, Reconnection-controlled decay of magnetohydrodynamic turbulence and the role of invariants, *Phys. Rev. X* **11**, 041005 (2021).
- [41] A. Brandenburg, K. Kamada, and J. Schober, Decay law of magnetic turbulence with helicity balanced by chiral fermions, *Phys. Rev. Res.* **5**, L022028 (2023).
- [42] G. Sigl and N. Leite, Chiral magnetic effect in protoneutron stars and magnetic field spectral evolution, *J. Cosmol. Astropart. Phys.* **01** (2016) 025.